FPGA-Based Optical Frequency Domain Reflectometry for Real-Time Fiber Shape Sensing

Cailing Fu, Wenfa Liang, Shijie Li, Rongyi Shan, Huajian Zhong, Shizhu Sun, Yanjie Meng, Weijia Bao, Yongzheng Xu, and Yiping Wang, *Senior Member, IEEE, Fellow, Optica*

***Abstract*—A real-time fiber shape sensing system using a field-programmable gate array (FPGA) in an optical frequency domain reflectometry (OFDR) was firstly demonstrated. At a spatial resolution of 10 mm, the refresh rates for strain demodulation based on weak fiber Bragg grating array (WFBGA) inscribed multicore fiber (MCF) using parallel computing and serial computing were 30 and 17 Hz, respectively. Here, a multi-channel data caching DDR4 module, a large-point fast Fourier transform module and a wavelength shift calculation module were designed and transplanted into the FPGA to achieve fast strain demodulation for shape sensing. And the strain accuracy of serial computing was higher than that of parallel computing due to the maximum sliding window sizes of 8192 and 2048 for serial computing and parallel computing after zero padding. Under the curvature radii of 15.0, 12.5, 10.0, 7.5, 5.0 cm and infinite, the root mean square errors (RMSEs) using serial computing were 0.2831, 0.2760, 0.1529, 0.1323, 0.1869, and 0.1806 cm, respectively, corresponding to distribution volumes of 0.0084, 0.0048, 0.0043, 0.0118, 0.0098, and 0.0013 cm^3, respectively. And the 3D shape was also reconstructed with an RMSE of 0.5905 cm and distribution volume of 0.0011 cm^3.**

***Index Terms*—Field-programmable gate array, optical frequency domain reflectometry, shape sensor.**

Received 14 October 2025; revised 24 December 2025; accepted 31 January 2026. Date of publication 4 February 2026; date of current version 2 May 2026. This work was supported in part by the National Natural Science Foundation of China under Grant U22A2088, Grant 62375178, and Grant 62405196, in part by Shenzhen Science and Technology Program under Grant JCYJ20220818095800001 and Grant JCYJ20241202124226032, in part by the LingChuang Research Project of China National Nuclear Corporation under Grant CNNC-LCKY-202265, and in part by China Postdoctoral Science Foundation under Grant GZC20231715 and Grant GZC20231719. *(Corresponding author: Yiping Wang.)*

The authors are with the Shenzhen Key Laboratory of Photonic Devices and Sensing Systems for Internet of Things, Guangdong and Hong Kong Joint Research Centre for Optical Fibre Sensors, State Key Laboratory of Radio Frequency Heterogeneous Integration, Shenzhen University, Shenzhen 518060, China, and also with the Shenzhen Key Laboratory of Ultrafast Laser Micro/Nano Manufacturing, Key Laboratory of Optoelectronic Devices and Systems of Ministry of Education/Guangdong Province, College of Physics and Optoelectronic Engineering, Shenzhen University, Shenzhen 518060, China (e-mail: fucailing@szu.edu.cn; 2210452035@email.szu.edu.cn; 2400233043@mails.szu.edu.cn; 1723118328@qq.com; 2250453001@email.szu.edu.cn; 2400233041@mail.szu.edu.cn; mengyanjie2020@email.szu.edu.cn; wjbao@szu.edu.cn; xuyongzheng@szu.edu.cn; ypwang@szu.edu.cn).

This article has supplementary downloadable material available at http://doi.org/10.1109/JLT.2026.3661104, provided by the authors.

This article has supplementary material provided by the authors and color versions of one or more figures available at https://doi.org/10.1109/JLT.2026.3661104.

Digital Object Identifier 10.1109/JLT.2026.3661104

I. Introduction

FIBER optic shape sensing (FOSS) has attracted attention in the medical field due to its ability to track the shape and position of dynamic objects, i.e., minimally invasive surgical continuous robots [1], navigation flexible instruments [2] and without visual contact. Fiber Bragg gratings (FBGs) with different resonant wavelengths, i.e., wavelength division multiplexing FBGs, were often used to realize shape sensing, where the measurement rate could reach hundreds of Hz [3], [4], [5]. However, the limited number of multiplexed gratings, i.e., limited sensing length, and lower sensing spatial resolution limit its further application in shape sensing. In contrast, FOSS based on optical frequency domain reflectometry (OFDR) has become one of the most promising method due to its high sensing spatial resolution and high sensitivity [6]. As we know, real-time and high spatial resolution demodulation of shape changes in navigation flexible instruments is a key factor related to whether this technology could be applied in the medical field [7]. However, the higher the spatial resolution, the more cycles of the cross-correlation operation. Thus, the computational load of the OFDR system is undoubtedly increased, thereby prolonging the demodulation time. To improve the demodulation rate of the OFDR, various methods based on graphics processor unit (GPU) and field programmable gate array (FPGA) have been demonstrated [8], [9], [10], [11], [12]. For example, a real-time OFDR strain system based on (GPU) with a demodulation rate of 60 Hz and lower strain resolution, i.e., the number of padding zeros was less than 1350, was demonstrated [8]. And a fast shape reconstruction OFDR system that employs GPU to parallelly calculate the cross-correlation wavelength shift of the multicore fiber (MCF) was proposed, and the time consumption was reduced by 21 times [9]. On the other hand, a OFDR strain system using FPGA as the hardware circuit to complete the calculation task was proposed, where the demodulation rate was accelerated by 21 times, i.e., 10 Hz under the spatial resolution of 30 cm [10]. Subsequently, a high-speed strain demodulation system employing a 2D FFT and frequency-domain cross-correlation algorithm based on FPGA was also proposed, where the real-time demodulation rate of 24 Hz. And the spatial resolution was 6.4 mm for 50 m test fiber [11]. In addition, a real-time and high spatial resolution OFDR strain sensing system that entirely employs FPGA for data acquisition and cross-correlation shift calculation was further demonstrated [12]. However, there

are still significant differences between the reported performance index and actual application requirements in the medical filed.

In this letter, a real-time and high-spatial-resolution OFDR distributed shape sensing system using WFBGA-inscribed MCF was demonstrated. The system was fully employing FPGA for strain demodulation with a refresh rate of 17 Hz and spatial resolution of 10 mm using serial computing. Among them, 2D-FFT, multi-channel data caching, data separation module, and wavelength shift calculation module were combined to achieve three cores strain demodulation. The resource consumption percentage of strain demodulation using parallel computing and serial computing in FPGA was compared. The 2D and 3D shape sensing property, including RMSE and stability, was further investigated using serial computing.

II. Experimental Setup and Methods

An OFDR system consisting of three main interferometers (MIs), i.e., MI_1, MI_2, and MI_3, was constructed to achieve real-time fiber shape sensing, which were independently connected to the two outer cores, i.e., Core5 (C_5), Core6 (C_6), and central cores, i.e., Core1 (C_1), of MCF, through fan in/out, as shown in Fig. 1(a). Note that the C_5 and C_6 were used to calculate the bending orientation and curvature based on the vector projections method [13]. And the C_1 was used to compensate the influences of external temperature and axial force by subtracting its wavelength shift [14]. A 60 cm-long MCF with femtosecond-laser-inscribed WFBGAs, i.e., WFBGA-inscribed MCF, was used in the experiment, where the length and space of the WFBG was 2 mm and 8 mm, respectively [15]. And the amplitude of the C_1, C_5 and C_6 was illustrated in Fig. 1(b). Then the Rayleigh backscattering (RBS) signals from three cores could be collected simultaneously in one frequency sweep of a tunable laser source (TLS). Compared with the use of optical switch method [13], the time required for frequency sweep was reduced. The light from a TLS (TLB-8800 Newport) was evenly divided into four parts by the optical coupler (OC_1), which entered MI_1, MI_2, MI_3, and auxiliary interferometer (AI), respectively. The AI, i.e., Michelson interferometer, was consisted of two Faraday rotating mirrors (FRMs) and a 20 m long delay fiber, which was used for providing an external clock to trigger data acquisition and collect MI signal at a uniform optical frequency. The light entering the MI1 was split two parts by OC_3 with a splitting ratio of 10:90, and entered the polarization controller (PC) and the C_1 of MCF, respectively, then mixed by OC_4. Two polarization beam splitters (PBSs), i.e., PBS_1 and PBS_2, were used to separate the collected interference signal into P-polarization and S-polarization, and were detected by two balanced photodetectors (BPDs), i.e., BPD_2 and BPD_3, respectively. The MI_2 and MI_3, which have the same structure as MI_1, were used to collect RBS signals from C_5 and C_6, respectively. Moreover, the FPGA board was equipped with FPGA chip analog-to-digital conversion (ADC) chip (four channels, 1 GBPS, 16 bit), and double data rate (DDR) chip, which is used to achieve fast strain demodulation for shape sensing.

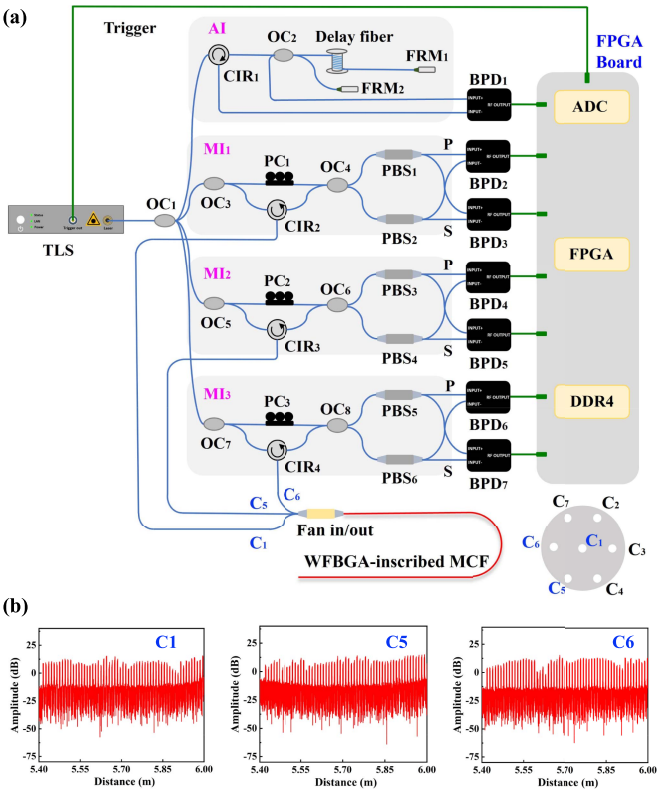

Fig. 1. (a) Experimental setup for real-time shape sensing using FPGA-based OFDR with weak fiber Bragg grating array (WFBGA) -inscribed multicore fiber (MCF). Note that the core combination of Core1 (C_1), Core5 (C_5), and Core6 (C_6) was selected to reconstruct the 2D and 3D shape. TLS: tunable laser source; OC: coupler; CIR: circulator; FRM: faraday rotating mirror; PC: polarization controller; PBS: polarization beam splitter; BPD: balanced photo-detector; AI: auxiliary interferometer; MI: main interferometer; (b) distance domain spectra of femtosecond-laser-inscribed WFBGA in C_1, C_5, and C_6 of 60 cm-long MCF, where the length and space of the WFBG was 2 mm and 8 mm, respectively.

To achieve real-time shape sensing, the strain demodulation process of C_1, C_5, and C_6 in WFBGA-inscribed MCF was transplanted into FPGA board. As shown in Fig. 2, the beat frequency signals of C_1, C_5, and C_6 with straight and curved shapes were firstly collected simultaneously by the ADC, corresponding to the reference (Ref.) signal and the measurement (Mea.) signal, respectively. Take C_1 as an example, the framework is the same as Ref. [12], including row 2-dimensional fast Fourier transformation (2D-FFT), column 2D-FFT, multi-channel data caching, i.e., writing/reading in MEMORY BLOCK0, MEMORY BLOCK1 and MEMORY BLOCK2, multiplying by twiddle factor. Note that the order of reading data from MEMORY BLOCK0, MEMORY BLOCK1 and MEMORY BLOCK2 is column, row, and column first, respectively. The same processes as described above were also exerted on C_5 and C_6. Currently, the Ref. and Mea. distance domain spectra of C_1, C_5 and C_6 could be obtained. Subsequently, a data separation module was designed to separate the Ref. and Mea. signals after MEMORY BLOCK2, synchronously extracting the position of each WFBG in the Ref. and Mea. signals through sliding window. Then the Ref. signal output through RD-Column was cached in MEMORY

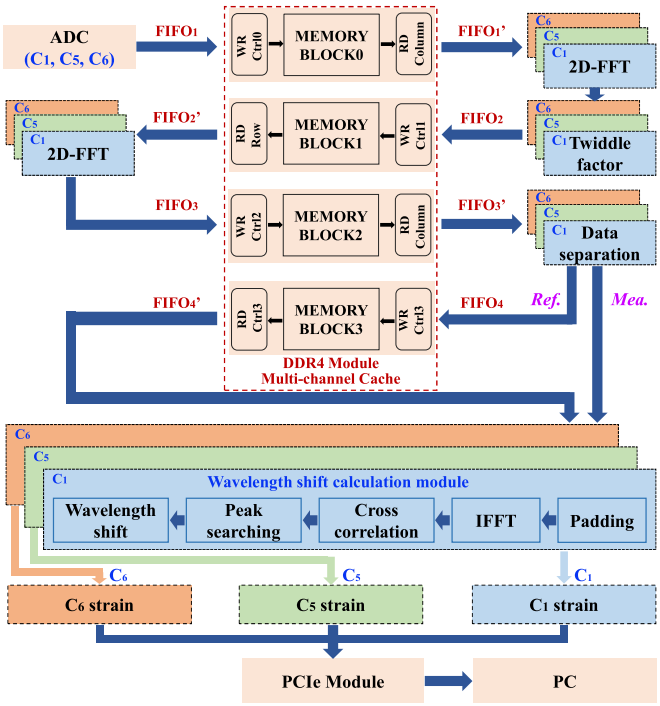

Fig. 2. Data processing flowchart of strain demodulation of C_1, C_5, and C_6 in WFBGA-inscribed MCF for shape sensing using FPGA board. ADC: analog-to-digital conversion; FIFO: first in first out; 2D-FFT: 2-dimensional fast Fourier transformation; Ref.: reference signal; Mea.: measurement signal; IFFT: inverse FFT; DDR: double data rate. PCIe: peripheral component interconnect express; PC: personal computer.

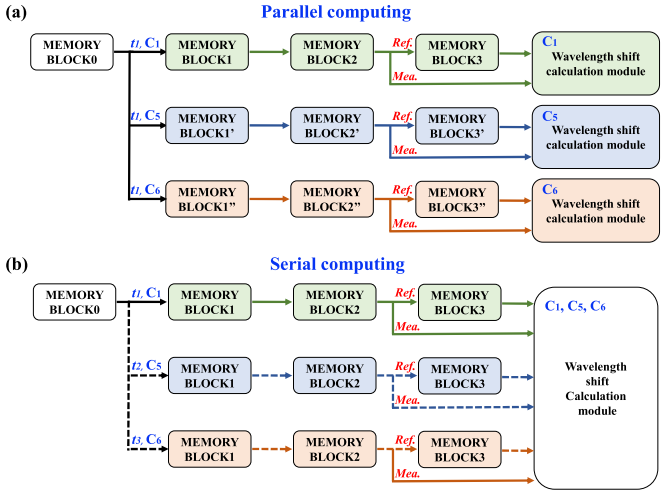

Fig. 3. Flow charts of two processing frameworks in FPGA, i.e., (a) parallel computing and (b) serial computing, corresponding to simultaneous and time-division processing of C_1, C_5, and C_6 beat signals.

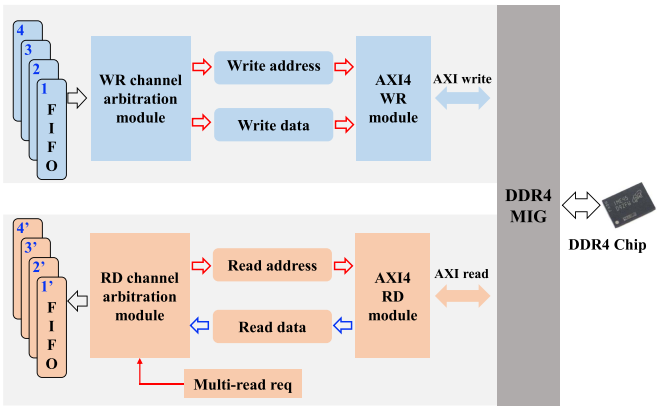

Fig. 4. Structure diagram for implementing multi-channel cache, i.e., multi-channel read/write, using DDR4 chip.

BLOCK3 and directly output, reducing once RD-column operation [12]. Then the distance domain of Ref. and Mea. signals were simultaneously input to the wavelength shift calculation module, including padding zero, inverse FFT (IFFT), cross-correlation, peaking searching operation. In this way, the strain distributions of C_1, C_5 and C_6 could be demodulated based on the calculated spectral shift, and then transmit to personal computer (PC) through peripheral component interconnect express (PCIe) module to reconstruct the 2D and 3D shape.

According to the strain demodulation flowchart in Fig. 2, two data processing frameworks, i.e., parallel computing and serial computing, were designed to compare their refresh rates. In parallel computing, the beat frequency signals of C_1, C_5, and C_6 were simultaneously and synchronously passed through MEMORY BLOCKs 1, 2, 3, and wavelength shift calculation module at time t_1, as shown in Fig. 3(a). On the contrary, the beat frequency signals of C_1, C_5, and C_6 were time-division processed at times t_1, t_2, and t_3, respectively, for serial computing, as shown in Fig. 3(b). Moreover, the process of implementing multi-channel caching in DDR4 module was illustrated in Fig. 4. The data written from different channels were firstly cached in different FIFOs, i.e., $FIFO_1$, $FIFO_2$, $FIFO_3$, and $FIFO_4$, and then written to the WR channel arbitration module. Each channel data was packaged and allocated a memory address, and then cached separately in the write data and write address. Subsequently, the data and address were converted into AXI write protocol frames through AXI4 WR module, transmitted to the DDR4 MIG module, and then written to the DDR4 chip. At the same time, a multi-read request instruction was sent to the RD channel arbitration module. The number of channels and data were identified, and the corresponding read address was sent to AXI4 RD module. Then the data was read from DDR4 chip, returned to RD channel arbitration module, and output to $FIFO_1$', $FIFO_2$', $FIFO_3$', and $FIFO_4$'.

The consumption percentages of resource in FPGA for strain demodulation using parallel computing and serial computing were investigated and compared. As shown in Fig. 5(a), the consumption percentages of look-up table (LUT), LUT random access memory (LUTRAM), flip-flops (FF), block random access memory (BRAM), digital signal processing (DSP), input and output (IO) were 54.30, 26.03, 48.53, 93.47, 22.77 and 43.11, respectively, using parallel computing, when the total data size was 1.0 MS, i.e., $D' = 1.0$ MS. And the maximum size of the sliding window after zero padding was 2048, i.e., $M = 2048$, for parallel computing, due to the 93.47% resource consumption of BRAM. Moreover, the refresh rate of 30 Hz was achieved using

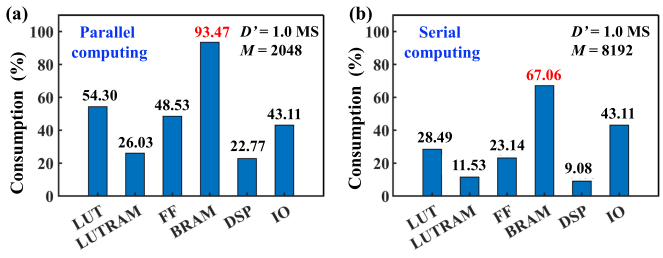

Fig. 5. Consumption percentages of in FPGA for strain demodulation using (a) parallel computing and (b) serial computing under the total data size of 1 MS, i.e., D' = 1.0 MS. Note that maximum size of the sliding window after zero padding for parallel and serial computing was 2048 and 8192, corresponding to refresh rates of 30 and 17 Hz, respectively.

TABLE I
PERFORMANCE COMPARISON OF OFDR BASED ON GPU AND FPGA

Processing unit	Sensing type	Sensing length	Spatial resolution	Size after zero padding	Refresh rate
GPU	Strain[8]	200 m	20 cm	1350	60 Hz
	Shape[9]	47.1 cm	5 mm	16384	\
FPGA	This work	60 cm	10 mm	2048	30 Hz
				8192	17 Hz

parallel computing, which was close to the repetitive sweeping frequency of TLS, as shown in Supplementary video S1.

Compared with parallel computing, the consumption percentages of LUT, LUTRAM, FF, BRAM, DSP, IO were reduced to 28.49, 11.53, 23.14, 67.06, 9.08, and 43.11, respectively, using serial computing, as shown in Fig. 5(b). And the maximum size of the sliding window after zero padding was improved to 8192, i.e., $M = 8192$. Compared to padding zero to 2048, a higher strain accuracy of 3.49 $\mu\varepsilon$ was exhibited after zero padding to 8192 [11]. In other words, the strain accuracy of serial computing was higher than that of parallel computing. However, the refresh rate was reduced to 17 Hz for serial computing, as shown in Supplementary video S2. Therefore, shape reconstruction in the subsequent experiment was carried out using serial computing in consideration of real-time and high strain accuracy. As we known, the data processing rate for distributed sensing could be effectively accelerated by the parallel computing in GPU, attributing to its large number of parallel computing units. As shown in Table I, the refresh rate was 60 Hz for GPU-based strain sensing [8]. However, there is no refresh rate was reported for GPU-based shape sensing [9]. In this work, the FPGA-based OFDR using parallel computing and serial computing with refresh rates of 30 and 17 Hz, respectively. To our knowledge, this is the first time to achieve real-time fiber shape sensing using FPGA-based OFDR with WFBGA-inscribed MCF.

III. EXPERIMENTAL RESULTS AND DISCUSSION

To verify the performance of the FPGA-based OFDR, the 2D and 3D shape sensing properties of WFBGA-inscribed MCF were further investigated using the combination of C_1, C_5, and C_6 based on serial computing. Similarly, the WFBGA-inscribed MCF was firstly placed on curvature plate with radii of 15.0,

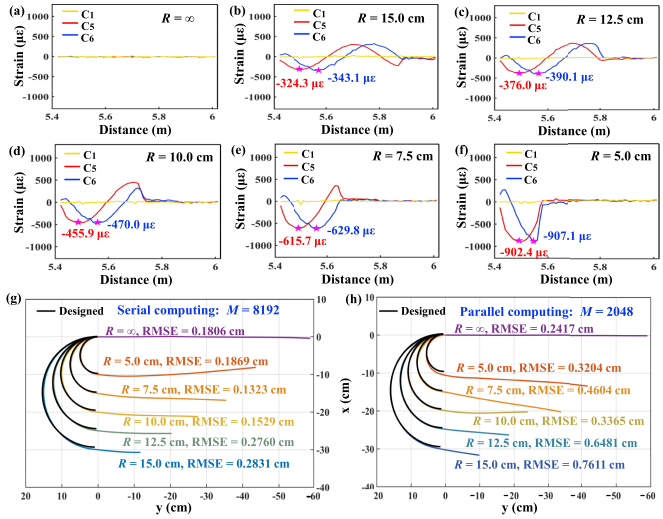

Fig. 6. Demodulated strain distributions of C1, C5, and C6 for the WFBGA-inscribed MCF using parallel computing, when the curvature radius was (a) infinite, (b) 15.0, (c) 12.5, (d) 10.0, (e) 7.5, and (f) 5.0 cm, respectively; reconstructed 2D shapes using (g) serial computing and (h) parallel computing, respectively.

12.5, 10.0, 7.5, and 5.0 cm, respectively [15]. To minimize the torsion introduced by operation as much as possible, one end of the MCF connected to FIFO was fixed, and the other end was attached with transparent tape. Then the end with transparent tape was moved to different curvature grooves. In the process, the transparent tape with MCF and the curvature groove were kept in the same plane. As shown in the yellow curves of Fig. 6(a)–(f), the demodulated strain of the C_1 at the geometric center was approximately 0 $\mu\varepsilon$, independent of the curvature radius. When the WFBGA-MCF was bent, the strain distribution of the outer cores, i.e., C_5 and C_6, exhibited a sinusoidal curve, labeled by red and blue curves, respectively. And the demodulated maximum strains of C_5 and C_6 were -324.3, -376.0, -455.9, -615.7, -902.4 $\mu\varepsilon$ and -343.1, -390.1, -470.0, -629.8, -907.1 $\mu\varepsilon$, respectively, when the curvature radius was 15.0, 12.5, 10.0, 7.5, and 5.0 cm, respectively. Obviously, the maximum strain of the outer core was increased as the curvature radius decreased. Using the vector projection method based on Bishop framework and afore-calculated strain, the reconstructed 2D fiber shapes of the bent segment were agreed well with the designed curvature radii, as shown in Fig. 6(g). In addition, the reconstructed length of WFBGA-inscribed MCF was 60 cm under the straight state, i.e., $R = \infty$, which was consistent with the actual length. Under the curvature radii of 15.0, 12.5, 10.0, 7.5, 5.0 cm and infinite, the root mean square errors (RMSEs) between the reconstructed and designed curvature radius were 0.2831, 0.2760, 0.1529, 0.1323, 0.1869, and 0.1806 cm, respectively. Note that the calculation of RMSE was only in the curvature segment. Besides, RMSE was calculated using other core combinations, i.e., C_{135}, with RMSE of 0.3104, 0.2650, 0.3170, 0.3583, and 0.4289 cm for curvature radii of 15.0, 12.5, 10.0, 7.5, and 5.0 cm, respectively. Obviously, the RMSE of the C_{156} combination was superior to that of C_{135}. Thus, the RMSE was further calculated based on C_{156} combination with parallel computing, as shown in Fig. 6(h). Obviously, the RMSEs were deteriorated to 0.7611,

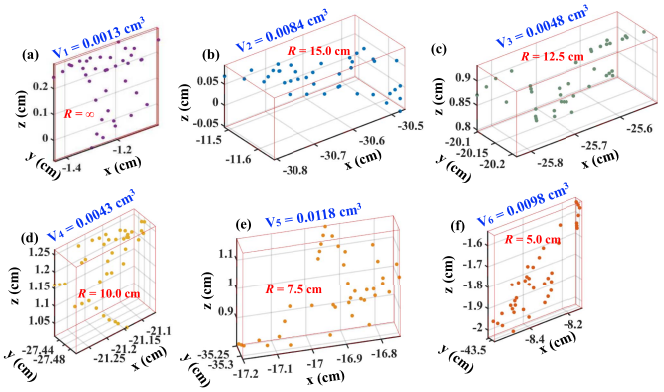

Fig. 7. The coordinate distribution of the end position of WFBGA-MCF at 40 repetitions under curvature radii of (a) infinite, (b) 15.0, (c) 12.5, (d) 10.0, (e) 7.5, and (f) 5.0 cm, respectively.

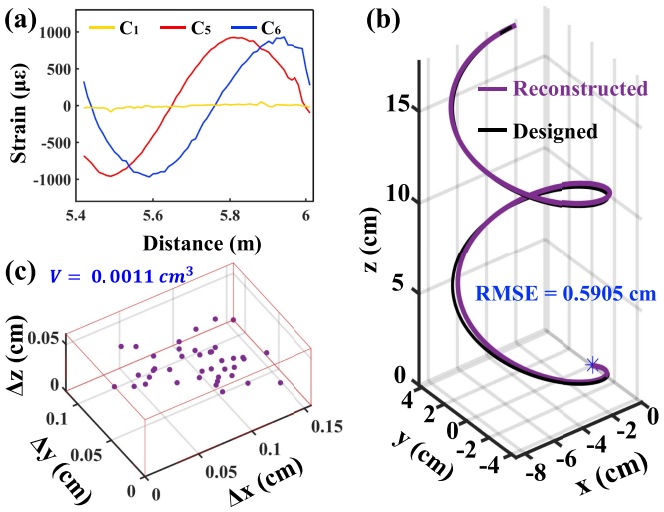

Fig. 8. (a) Obtained strain distribution of C_1, C_5, and C_6 for the WFBGA-MCF; (b) reconstructed 3D spiral shape of; (c) coordinate distribution of the end position of WFBGA-MCF.

0.6481, 0.3365, 0.4604, 0.3204, and 0.2417 cm, respectively. This further indicated that the strain accuracy of reconstructed shapes using serial computing was better than that of parallel computing, due to the maximum size of the sliding window after zero padding in serial and parallel computing being 2048 and 8192, respectively.

To further verify the stability of FPGA-based OFDR shape reconstruction, the distribution of end position was studied under the same curvature and repeated 40 times. Note that the calculation of stability was in consideration of the entire WFBGA-inscribed MCF. As shown in Fig. 7(a), the coordinates of the end position were fall within a rectangular prism with a volume of 0.0013 cm^3, when the curvature radius was infinite, i.e., $R = \infty$. The volumes were 0.0084, 0.0048, 0.0043, 0.0118, and 0.0098 cm^3 under the curvature radii of 15.0, 12.5, 10.0, 7.5, and 5.0 cm, respectively, as shown in Fig. 7(b)–(f). Compared with the bent state, the distribution volume in the straight state was the smallest, which may be due to the smallest MCF torsion in the straight state. Moreover, the instability of the end position was mainly distributed in the x-axis and z-axis directions. In addition, the RMSE and stability of the reconstructed shape were independent of each other.

When the WFBGA-MCF was placed on a spiral groove [15], the tendency of the strain distribution of C_1, C_5, and C_6 was similar as the 2D shape, as shown in Fig. 8(a). In the 3D shape sensing, the MCF was wound into a circle with a diameter of 8.7 cm on the plane using afore-method in the 2D shape sensing, and then raised to 3D spiral. And the MCF should be as close to the groove as possible without lifting and twisting it to reduce the torsion on the demodulated strain. And the reconstructed 3D shape using serial computing was also very consistent with the designed spiral curve with an RMSE of 0.5905 cm, which was larger than that of 2D shape, as shown by the purple and black curves in Fig. 8(b). The real-time 3D shape sensing using FPGA-based OFDR with serial computing was illustrated in Supplementary video S3. Similarly, the distribution volume of the end position repeated 40 times was 0.0011 cm^3, as shown in Fig. 8(c).

IV. Conclusion

In conclusion, to our knowledge, this is the first time to achieve real-time fiber shape sensing using FPGA-based OFDR with WFBGA-inscribed MCF. A real-time, i.e., 30 Hz, and high-spatial-resolution, i.e., 10 mm, OFDR distributed shape sensing system that entirely employs FPGA with WFBGA-inscribed MCF for strain demodulation was demonstrated. The refresh rates for strain demodulation using parallel computing and serial computing were 30 and 17 Hz, corresponding to the consumption percentages of BRAM of 93.47 and 67.06, respectively. Due to the maximum size of the sliding window after zero padding being 2048 and 8192, the strain accuracy of serial computing was higher than that of parallel computing. Under the curvature radii of 15.0, 12.5, 10.0, 7.5, 5.0 cm and infinite, the obtained root mean square errors (RMSEs) using serial computing were 0.2831, 0.2760, 0.1529, 0.1323, 0.1869, and 0.1806 cm, respectively, corresponding to distribution volumes of 0.0084, 0.0048, 0.0043, 0.0118, 0.0098, and 0.0013 cm^3, respectively. The 3D shape was also reconstructed with an RMSE of 0.5905 cm and distribution volume of 0.0011 cm^3. The RMSEs for 2D and 3D shape sensing could be further optimized through spun MCF.

References

[1] C. Shi et al., "Shape sensing techniques for continuum robots in minimally invasive surgery: A survey," *IEEE Trans. Biomed. Eng.*, vol. 64, no. 8, pp. 1665–1678, Aug. 2017.

[2] S. Jaeckle et al., "Fiber optical shape sensing of flexible instruments for endovascular navigation," *Int. J. Comput. Assist. Radiol. Surg.*, vol. vol. 14, no. 12, pp. 2137–2145, Dec. 2019, doi: 10.1007/s11548-019-02059-0.

[3] D. Paloschi, K. A. Bronnikov, S. Korganbayev, A. A. Wolf, A. Dostovalov, and P. Saccomandi, "3D shape sensing with multicore optical fibers: Transformation matrices versus Frenet-Serret equations for real-time application," *IEEE Sensors J.*, vol. 21, no.no. 4, pp. 4599–4609, Feb. 2021, doi: 10.1109/JSEN.2020.3032480.

[4] Y. Tian et al., "Optical fiber shape reconstruction algorithm based on 3D Euler spiral model," *Meas. Sci. Technol.*, vol. 35, no. 11, Nov. 2024, Art. no. 115111, doi: 10.1088/1361-6501/ad6e0b.

[5] K. Bronnikov et al., "Durable shape sensor based on FBG array inscribed in polyimide-coated multicore optical fiber," *Opt. Exp.*, vol. 27, no. 26, pp. 38421–38434, Dec. 2019, doi: 10.1364/OE.380816.
[6] C. Shao et al., "OFDR with local spectrum matching method for optical fiber shape sensing," *Appl. Phys. Exp.*, vol. 12, no. 8, Aug. 2019, Art. no. 082010, doi: 10.7567/1882-0786/ab3107.
[7] S. Li et al., "Twist compensated, high accuracy and dynamic fiber optic shape sensing based on phase demodulation in optical frequency domain reflectometry," *Mech. Syst. Signal Process.*, vol. 216, Jul. 2024, Art. no. 111462, doi: 10.1016/j.ymssp.2024.111462.
[8] C. Wang et al., "GPU-based real-time distributed dynamic strain sensing in optical frequency domain reflectometry," *IEEE Sensors J.*, vol. 21, no. 21, pp. 24166–24176, Nov. 2021, doi: 10.1109/JSEN.2021.3114556.
[9] R. Y. Shan et al., "Fast shape reconstruction based on GPU parallel computation in optical frequency domain reflectometry," *IEEE Sensors J.*, vol. 24, no. 21, pp. 34591–34597, Nov. 2024, doi: 10.1109/JSEN.2024.3462463.
[10] W. Q. He et al., "Real-time performance improvement approach based on FPGA in OFDR system," *Opt. Fiber Technol.*, vol. 75, Jan. 2023, Art. no. 103212, doi: 10.1016/j.yofte.2022.103212.
[11] H. M. Wang et al., "Real-time sensing approach for optical frequency domain reflectometry using an FPGA-based high-speed demodulation algorithm," *Opt. Exp.*, vol. 32, no. 19, pp. 33247–33261, Sep. 2024, doi: 10.1364/OE.537627.
[12] W. F. Liang et al., "Real-time distributed strain sensing using FPGA-based optical frequency domain reflectometry," *IEEE Trans. Instrum. Meas.*, vol. 74, Nov. 2024, Art. no. 7000608, doi: 10.1109/TIM.2024.3502767.
[13] Y. J. Meng et al., "Shape sensing using two outer cores of multicore fiber and optical frequency domain reflectometer," *J. Lightw. Technol.*, vol. 39, no. 20, pp. 6624–6630, Oct. 2021, doi: 10.1109/JLT.2021.3100854.
[14] F. Khan, A. Denasi, D. Barrera, J. Madrigal, S. Sales, and S. Misra, "Multi-core optical fibers with Bragg gratings as shape sensor for flexible medical instruments," *IEEE Sensors J.*, vol. 19, no. 14, pp. 5878–5884, Jul. 2019, doi: 10.1109/JSEN.2019.2905010.
[15] C. L. Fu et al., "OFDR shape sensor based on a femtosecond-laser-inscribed weak fiber Bragg grating array in a multicore fiber," *Opt. Lett.*, vol. 49, pp. 1273–1276, Mar. 2024, doi: 10.1364/OL.516067.

Cailing Fu was born in Hubei, China, in 1989. She received the M.S. degree in optical engineering from the Wuhan University of Technology, Wuhan, China, in 2015, and the Ph.D. degree in optical engineering from Shenzhen University, Shenzhen, China, in 2018. From 2018 to 2020, she was with information and communication engineering of Shenzhen University, as a Postdoc Research Fellow. Since 2020, she has been an Assistant Professor and Associate Professor with Shenzhen University. Her current research interests include distributed optical fiber sensing technology and fiber shape sensing.

Wenfa Liang was born in Guangdong, China, in 1999. He received the bachelor's degree from the Dongguan University of Technology, Dongguan, China, in 2018 and the master's degree from Shenzhen University, Shenzhen, China, in 2025. His research interests include signal demodulation based on FPGA and fiber optic shape sensing.

Shijie Li was born in Guangdong, China. He received the bachelor's degree from Shenzhen University, Shenzhen, China, in 2024. His research interests include signal demodulation based on FPGA and fiber optic shape sensing.

Rongyi Shan was born in Guangdong China, in 1999. He received the B.S. degree from the Guangdong University of Technology, Guangzhou, China, in 2022. His current research focuses on distributed optical sensing.

Huajian Zhong was born in Jiangxi, China, in 1998. He received the B.S. degree from the Changchun University of Science and Technology, Changchun, China, in 2020, and the Ph.D. degree in optical engineering from Shenzhen University, Shenzhen, China, in 2025. His current research focuses on distributed optical sensing.

Shizhu Sun was born in Jiangxi, China. He received the master's degree from Jiangxi Normal University, Nanchang, China, in 2024. His current research focuses on fabrication of multicore fiber grating.

Yanjie Meng was born in Guangling, China, in 1994. He received the M.S. degree from the China University of Mining and Technology, Xuzhou, China, in 2019, and the Ph.D. degree in optical engineering from Shenzhen University, Shenzhen, China, in 2023. His research interests include optical fiber shape sensing and femtosecond laser processing.

Weijia Bao received the B.S. degree in electronic information science and technology from Xidian University, Shaanxi, China, in 2013, and the Ph.D. degree in optics from Northwest University, Xi'an, China, in 2018. He is currently an Assistant Professor with the College of Physics and Optoelectronic Engineering, Shenzhen University, Shenzhen, China. His current research interests include fiber grating inscription, micromaching, and fiber sensing technology

Yongzheng Xu received the master's degree from Tianjin Polytechnic University, Nanchang, China, in 2016, and the Ph.D. degree from Shandong University, Jinan, China, in 2022. His research focuses on optical fiber shape sensing.

Yiping Wang (Senior Member, IEEE) was born in Chongqing, China, in 1971. He received the B.Eng. degree in precision instrument engineering from the Xi'an University of Technology, Xi'an, China, in 1995, and the M.S. and Ph.D. degrees in optical engineering from Chongqing University, Chongqing, China, in 2000 and 2003, respectively. From 2003 to 2005, he was with Shanghai Jiao Tong University, Shanghai, China, as a Postdoctoral Fellow. From 2005 to 2007, he was with The Hong Kong Polytechnic University, as a Postdoctoral Fellow. From 2007 to 2009, he was with the Leibniz Institute of Photonic Technology, Jena, Germany, as a Humboldt Research Fellow. From 2009 to 2011, he was with the Optoelectronics Research Centre, University of Southampton, Southampton, U.K., as a Marie Curie Fellow. Since 2012, he has been with Shenzhen University, Shenzhen, China, as a Distinguished Professor. He has authored or coauthored one book, 21 patent applications, and more than 240 journal and conference papers. His current research interests include optical fiber sensors, fiber gratings, and photonic crystal fibers. He is currently a senior member of the Optical Society of America and the Chinese Optical Society.